

# A Magnetic Analogue to the Isotope Effect by Raman Scattering in $(\text{CaLa})_1(\text{BaLa})_2\text{Cu}_3\text{O}_y$

Dirk Wulferding,<sup>1,2</sup> Meni Shay,<sup>3,4</sup> Gil Drachuck,<sup>3</sup> Rinat Ofer,<sup>3</sup> Galina Bazalitsky,<sup>3</sup> Zaher Salman,<sup>5</sup> Peter Lemmens,<sup>1</sup> and Amit Keren<sup>3</sup>

<sup>1</sup>*Institute for Condensed Matter Physics, Technical University of Braunschweig, D-38106 Braunschweig, Germany*

<sup>2</sup>*Center for Artificial Low Dimensional Electronic Systems,*

*Institute for Basic Science, 77 Cheongam-Ro, Nam-Gu,*

*Pohang 790-784, Korea and Department of Physics,*

*Pohang University of Science and Technology, Pohang 790-784, Korea*

<sup>3</sup>*Department of Physics, Technion - Israel Institute of Technology, Haifa 32000, Israel*

<sup>4</sup>*Department of Physics and Optical Engineering, Ort Braude College, 21982 Karmiel, Israel*

<sup>5</sup>*Laboratory for Muon Spectroscopy, Paul Scherrer Institute, 5232 Villigen PSI, Switzerland*

(Dated: February 28, 2014)

We present a Raman spectroscopic investigation of charge compensated antiferromagnetic  $(\text{Ca}_x\text{La}_{1-x})(\text{Ba}_{1.75-x}\text{La}_{0.25+x})\text{Cu}_3\text{O}_y$  single crystals. In this system  $x$  controls the interactions and  $y$  the doping. We determine the two-magnon Raman peak position  $E_{max}$ . In the absence of doping  $E_{max}$  is directly proportional to the superexchange strength  $J$ . We find that both  $x$  and  $y$  affect  $E_{max}$  considerably. The Raman measurements are accompanied by a muon spin rotation determination of the Néel temperature on the same samples, which confirm independently the strong dependence of the magnetic interaction on  $x$  and  $y$ . The Raman data reinforce the relation  $T_c^{max}(x) \propto J(x)$ , where  $T_c^{max}(x)$  is the maximum superconducting transition temperature for a given  $x$ . This result shows the importance of orbital overlap to cuprate superconductivity in the same way that changing isotopes clarified the importance of atomic mass to metallic superconductivity.

**PACS numbers:** 74.20.-z, 74.25.Ha, 74.72.Cj

The complexity of high temperature superconductors (HTSC), with several parameters controlling their properties, hinders progress in uncovering their superconducting mechanism. It is extremely difficult to isolate and control only one parameter at a time. This is contrasted by the metallic superconductors such as Hg, Sn, and Tl, where changing isotopes, for example, highlights the role of the atomic mass in setting their critical temperature. [1] To overcome the experimental challenge in the study of HTSC, we prepare and investigate single crystalline samples of the  $(\text{Ca}_x\text{La}_{1-x})(\text{Ba}_{1.75-x}\text{La}_{0.25+x})\text{Cu}_3\text{O}_y$  (CLBLCO) system, with  $x = 0.1$  and  $0.4$ . This system is isostructural to YBCO and has two tuning parameters: the amount of oxygen  $y$ , and the ratio of Calcium to Barium set by  $x$ . Each  $x$  defines a superconducting family. Calcium and Barium have the same valence and their total amount in the chemical formula is constant. Therefore,  $x$  does not serve as a formal dopant. However,  $x$  tunes the Cu-O-Cu bond distances and buckling angles, leading to variations in the overlap of orbitals. [2] This property of CLBLCO opens a window to investigate the relation between  $T_c$  and the physical parameters that are determined by orbital overlap.

Phase diagrams of CLBLCO with different  $x$  are shown in Fig. 1(a). They summarize muon spin rotation ( $\mu\text{SR}$ ) [3, 4] and transport [5] experiments performed on powder samples. It can be seen that the transition temperatures to the antiferromagnetic, spin glass, and su-

perconducting phases ( $T_N$ ,  $T_g$ , and  $T_c$ , respectively) are  $x$  dependent. In particular, the superconducting transition temperature of the optimally doped samples,  $T_c^{max}$ , varies by 30% from the  $x = 0.1$  to the  $x = 0.4$  family. However, high-resolution powder x-ray diffraction [6] and NMR experiments [7] indicate that  $x = 0.1$  samples are more ordered than  $x = 0.4$  ones. Therefore, disorder can not be responsible for the reduction of  $T_c^{max}$  as  $x$  decreases. There has to be a more fundamental reason for these variations of  $T_c^{max}$ .

Panel (b) of Fig. 1 depicts a re-scaled phase diagram for CLBLCO. We obtain this unified diagram by replacing  $T_N$  with the superexchange  $J$ , normalizing the temperature scales by  $T_c^{max}$ , [4] and transforming the oxygen composition parameter  $y$  according to  $\Delta n_{p\sigma} = \kappa(x) \cdot (y - y_N)$ . [8] The scaling parameter  $\kappa(x)$  translates to the doping efficiency with which holes are introduced into the  $\text{CuO}_2$  planes and was determined via measurements of the  $^{17}\text{O}$  nuclear quadrupole resonance parameter  $\nu_Q$ . [8]  $y_N$  is the oxygen composition where  $T_N$  starts to decrease, as shown in Fig. 1(b), and  $\Delta n_{p\sigma}$  stands for effective hole variation on the oxygen orbital. The unified phase diagram suggests a common origin for the magnetic and the superconducting phase transitions, namely,  $T_c \propto J$ . [4] The superexchange, in turn, is determined by orbital overlaps. In terms of the Hubbard model, a proportionality between  $T_c$  and  $J$  implies that cuprate superconductivity is driven by kinetic energy. [9]

However, the values for  $J$  were determined by  $\mu\text{SR}$ ,

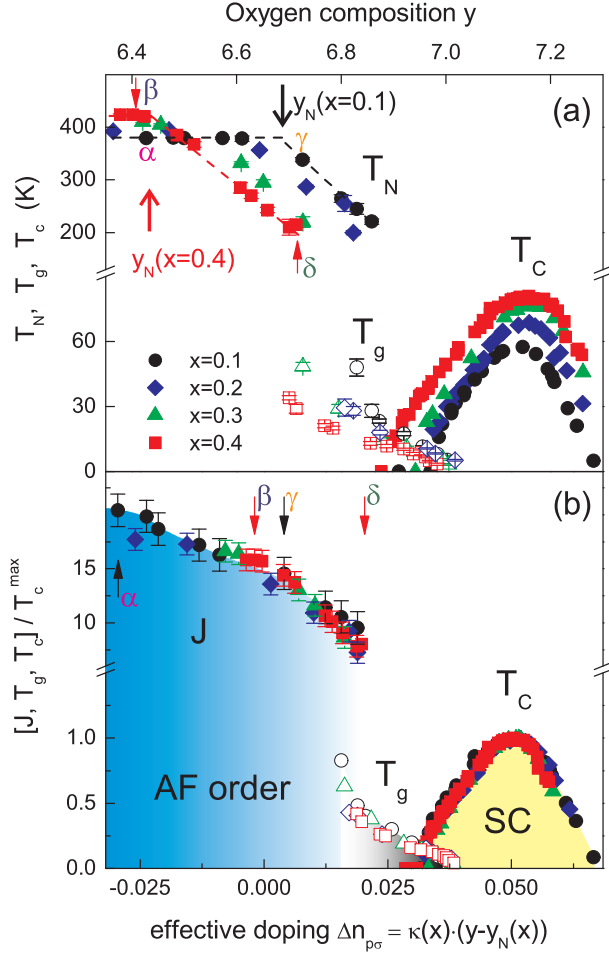


FIG. 1. (Color online) a) phase diagram of CLBLCO for the four families  $x=0.1, 0.2, 0.3$  and  $0.4$ .  $T_N$ ,  $T_g$  (open symbols) and  $T_c$  are plotted as function of oxygen composition  $y$ . The long arrows point to the  $y$  values where  $T_N$  starts to drop which defines  $y_N$ . b) displays  $J$  and the temperatures normalized by  $T_c^{\max}$  as function of doping variation  $\Delta n_{p\sigma}$ .  $\alpha - \delta$  indicate the positions of the four samples in the phase diagram.

which suffers from a serious drawback; it involves measurements over a wide range of temperatures in which  $J$  could change due to lattice expansion. Furthermore, the theory that extracts  $J$  from the data is rather involved and can only fit the data to a certain extent. [4] The work presented here overcomes these challenges by using two-magnon Raman scattering experiments. This technique determines  $J$  directly by measuring the shift in the photon energy  $E_{\max}$  between incoming and outgoing light due to a spin flip process of two adjacent spins. We measure the Raman shift as a function of both  $x$  and  $y$  and confirm the intimate relation between  $T_c^{\max}$  and  $J$  found by  $\mu$ SR.

Single crystals of  $(\text{Ca}_x\text{La}_{1-x})(\text{Ba}_{1.75-x}\text{La}_{0.25+x})\text{Cu}_3\text{O}_y$  with  $x = 0.1$  and  $0.4$  were successfully grown in a floating zone furnace. [10] In order to control the amount of

oxygen in the sample we followed the procedure known for powder samples of this material. [5] The oxygen composition of the samples has been determined by iodometric titration. [10]

For the Raman measurements the crystals were cleaved to obtain a shiny, flat, virgin surface. The cleaving produces facets which are perpendicular to the  $c$ -axis. Therefore the light scatters with the polarization in the  $ab$  plane for all measurements. Polarized Raman spectra were obtained using a Jobin-Yvon micro-Raman spectrometer (LabRAM HR) in backscattering geometry with a  $\lambda = 532$  nm solid state Nd:YAG laser as a light source, a  $50\times$  magnification objective, followed by a notch filter and a diffraction grating with 1800 grooves/mm. The detection was done by a nitrogen cooled CCD (Horiba Spectrum One). To prevent damage to the sample from overheating the laser power at the sample was kept below 1 mW, using a neutral density filter. The samples were placed in a cold-finger cryostat with a temperature range of 5 – 400 K.

The CLBLCO system crystallizes in a simple tetragonal structure (space group  $P4/mmm$ ). Five Raman active phonon modes are expected from backscattering within the  $ab$  plane. Four of these phonon modes are of  $A_{1g}$  symmetry where the scattered light has the same polarization as the incident light. [10] One phonon mode has a  $B_{1g}$  symmetry, where the polarization of the scattered light  $\vec{e}_s$  is perpendicular to the incident light polarization  $\vec{e}_i$  and the phonon intensity reaches a maximum when both  $\vec{e}_i$  and  $\vec{e}_s$  are at  $45^\circ$  from the  $a$  and  $b$  axis. This intensity dependence allows for an easy orientation of the crystallographic  $ab$  plane.

In Fig. 2(a) we depict raw two-magnon Raman scattering data for four samples marked  $\alpha, \beta, \gamma, \delta$ . Peaks with energies below  $1500 \text{ cm}^{-1}$  are due to phonon and multi-phonon scattering. The position of these samples in the phase diagram is indicated in Fig. 1(a) and (b). Samples  $\alpha$  and  $\gamma$  are part of the  $x = 0.1$  family, while samples  $\beta$  and  $\delta$  belong to the  $x = 0.4$  family. In the unified phase diagram, Fig. 1(b), it can be seen that samples  $\beta$  and  $\gamma$  are comparable with respect to doping at  $\Delta n_{p\sigma} \approx 0$ , while sample  $\alpha$  is in the highly underdoped region and sample  $\delta$  is on the verge of the spin-glass phase. The data in Fig. 2(a) is taken at  $T = 20$  K, deeply in the magnetically ordered phase. The arrows in Fig. 2(a) indicate the peaks' respective maxima. A clear shift in the two-magnon peak energy is observed for the different samples. For both families the peak shifts to lower energies as  $y$  increases; in accordance with a previous Raman study. [11] As  $y$  approaches the spin glass phase, the two-magnon Raman signal loses dramatically in intensity and vanishes in the spin glass phase. At equal  $y$ , the  $x = 0.4$  sample has a higher two-magnon mode energy than the  $x = 0.1$  sample. The principle observation is that samples  $\beta$  and  $\gamma$ , with the same effective doping ( $\Delta n_{p\sigma}$ ) but varying  $x$ , exhibit a huge difference in the two-magnon

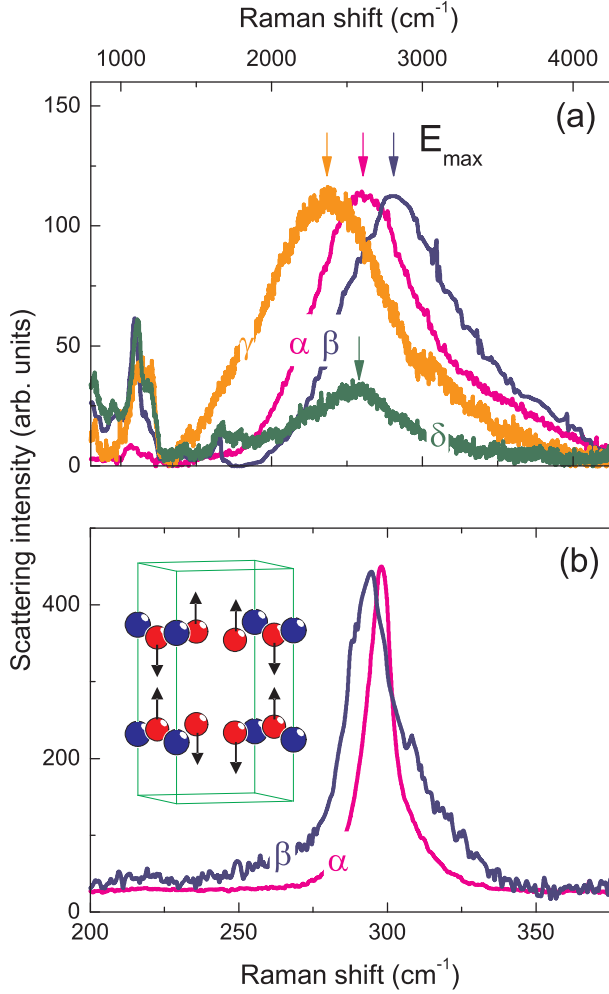


FIG. 2. (Color online) a) the two-magnon mode for samples  $\alpha - \delta$ , measured at  $T = 20$  K. b) compares the  $B_{1g}$  phonon mode of samples  $\alpha$  and  $\beta$ . The atomic displacement pattern for this phonon mode is indicated in the inset, the red and blue spheres correspond to oxygen and copper, respectively.

energy, with  $\beta$  being the largest.

In order to verify that the broad peak around  $2500 \text{ cm}^{-1}$  is indeed related to a two-magnon scattering process we measure its intensity as a function of temperature. The results for  $x = 0.1$   $y = 6.34$  are shown in Fig. 3(a). It is evident that the intensity of the peak drops above  $T_N = 375(2)$ . However, some remaining intensity of the two-magnon scattering is observed even at 400 K due to its local scattering nature. Moreover, as the temperature increases the peak shifts to lower energies, revealing the temperature dependence of  $E_{max}$ . At  $T \simeq T_N$  there is a high probability that neighbors of the spin-flipping pair are excited. This will reduce the energy cost in the flipping process. [12]

Fig. 3(b) shows the Raman spectra at four different polarizations. Here, we use the following notations:  $(xx) \hat{=} \vec{e}_i \perp \vec{e}_s \parallel a\text{-axis}$ ;  $(x'x') \hat{=} \vec{e}_i \perp \vec{e}_s \angle 45^\circ a\text{-axis}$ ;  $(x'y') \hat{=} \vec{e}_i \perp \vec{e}_s \angle 45^\circ b\text{-axis}$ ;  $(xy) \hat{=} \vec{e}_i \perp \vec{e}_s \parallel b\text{-axis}$ . It is found that the broad peak appears only in  $B_{1g}$  configuration, i.e. in  $(xx)$  and  $(x'y')$  polarization, as expected from two-magnon Raman scattering in a square lattice. [13, 14]

In Fig. 2(b) we plot the low energy part of the Raman spectra for samples  $\alpha$  and  $\beta$ , focussing on the  $B_{1g}$  phonon mode. The atomic displacement for this mode corresponds to an out-of-plane motion of oxygen ions in the  $\text{CuO}_2$  plane at  $\approx 300 \text{ cm}^{-1}$ . This motion is sketched in the inset of Fig. 2(b). We note two important observations regarding the phonons: *i*) no significant frequency shift occurs with changing  $x$ , and *ii*) the family with  $x = 0.1$  has a smaller line width. Both trends are independent of doping. In particular, the  $y$  dependence of the line width can be seen Fig. 4(a).

Observation *i*) supports the notion that phonons do not play a role in the superconducting mechanism for CLBLCO. The line width is a measure of the crystal quality and inverse proportional to the phonon life time. Thus, *ii*) suggests that the  $x = 0.1$  family offers the highest phonon coherence lengths. This is in agreement with the x-ray diffraction and NMR measurements of CLBLCO and reinforces the conclusion that crystal quality is not responsible for the variation in  $T_c^{max}$ .

Two of the samples that participated in the Raman measurements were subsequently optimally oxidized to  $y = 7.12$ . Their  $T_c^{max}$  was determined by magnetization measurements performed with a SQUID magnetometer. The data is plotted in Fig. 4(b). Here we note a variation between crystalline and powder samples: in the  $x = 0.1$  family, the  $T_c^{max}$  of the powder sample is  $\approx 3\%$  larger compared to the crystalline sample, while in the  $x = 0.4$  family the difference is as large as  $\approx 6\%$ . Nevertheless,  $T_c^{max}$  of the  $x = 0.4$  sample is much higher than that of the  $x = 0.1$  sample.

In light of the variations in  $T_c$  between powders and crystals it is important to check the antiferromagnetic part of the phase diagram. Thus, we measured  $T_N$  for all the samples that participated in the Raman experiments, using zero field  $\mu\text{SR}$ . In these experiments we follow the angular rotation frequency  $\omega$  of the spin of a muon implanted in the sample as a function of temperature.

The measurements were performed at the General Purpose Surface-Muon Instrument at the Paul Scherrer Institute (PSI). In Fig. 4(c) we depict the temperature dependent muon rotation frequency  $\omega$  for samples  $\alpha$ ,  $\beta$ , and  $\gamma$ . The Néel temperature is defined as the point where  $\omega \rightarrow 0$  upon warming. We find that the Néel temperatures of the crystal and the powder agree very well. In particular, as the oxygen composition increases (samples  $\alpha$  and  $\gamma$ )  $T_N$  decreases. At constant  $y$  (samples  $\alpha$  and  $\beta$ )  $T_N$  increases with  $x$ . And, most importantly, at constant effective doping (samples  $\beta$  and  $\gamma$ )  $T_N$  increases from 376 K at  $x = 0.1$  to 420 K at  $x = 0.4$ .

The scattering mechanism for a two-magnon process in an undoped sample corresponds to a simultaneous ex-

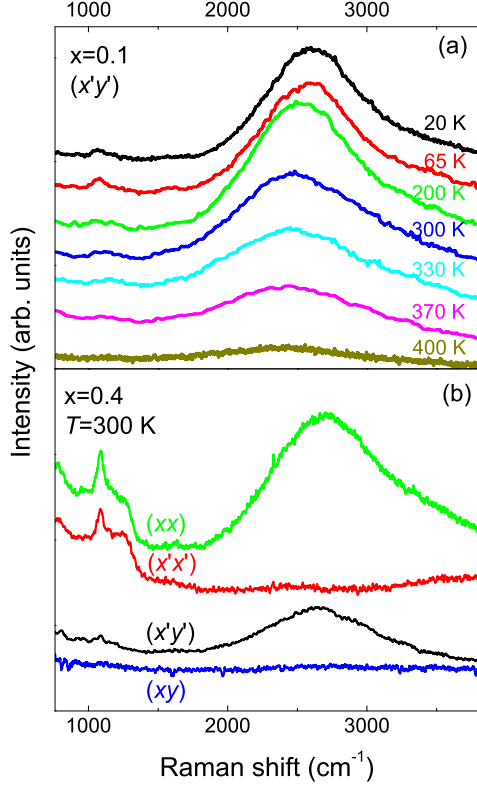


FIG. 3. (Color online) a) Temperature dependence of the two-magnon mode for the  $x = 0.1$  sample. b) Polarization dependence of the two-magnon mode measured at  $T = 300$  K.

change of two neighboring spins, induced by the incoming light. As a result, the magnetic coupling of the exchanged spins to their neighboring spins will be broken and photons with reduced energy will be emitted. Hence, the photon energy shift  $E_{max}$  is related to  $J$ . A simple broken bond counting argument for spin 1/2 on a two dimensional square lattice indicates that the Raman shift peaks at  $3J$ . More detailed calculation asserts that the exact factor between the Raman shift and  $J$  ranges from 2.71, [15] via 3.32, [16] to 3.38. [17] For the purpose of the work presented here it is sufficient to assume that the ratio between the Raman shift and  $J$  is similar to 3 and constant for all CLBLCO compounds. In a doped sample the number of broken bonds in the scattering process is smaller and  $E_{max}$  is expected to decrease with doping.

In Fig. 5 we compare the Raman shift  $E_{max}$  as function of oxygen composition  $y$  for the two families. The data points corresponding to samples  $\alpha - \delta$  are marked accordingly. For low  $y$  values, the  $x = 0.4$  samples have higher two-magnon mode energies than the  $x = 0.1$  samples. This result indicates that  $J$  is higher for the family with higher  $T_c^{max}$ . In both cases a clear and steady decrease is observed as a function of  $y$ . Around  $y = 6.8$

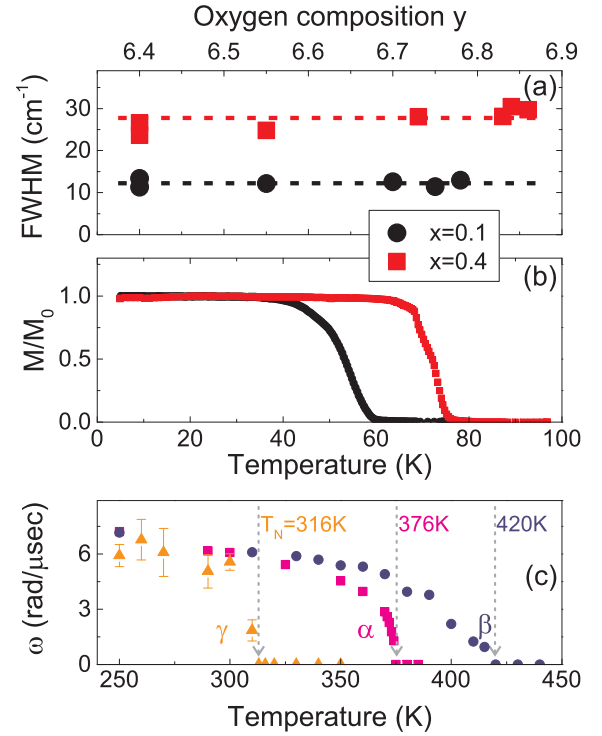


FIG. 4. (Color online) a) Full width at half maximum (FWHM) of the  $B_{1g}$  phonon mode at  $290 \text{ cm}^{-1}$  for both families as function of oxygen composition  $y$ . The lines are guides to the eyes. b) Magnetization as function of temperature for optimally doped samples of  $x = 0.1$  and  $x = 0.4$ . c) Néel temperature determined for the three samples  $\alpha$ ,  $\beta$ ,  $\gamma$  as indicated in the phase diagram using  $\mu\text{SR}$ .

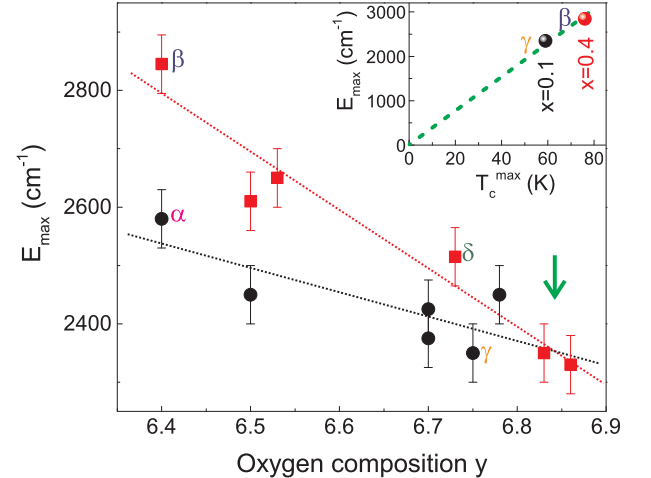


FIG. 5. (Color online) Doping dependence of the two-magnon mode energy  $E_{max}$  for the two families  $x = 0.1$  (black) and  $x = 0.4$  (red). The samples  $\alpha - \delta$  are indicated. The green arrow denotes the crossing point. Inset:  $E_{max}$  measured for the  $\Delta n_p \simeq 0$  samples  $\gamma$  and  $\beta$ , as function of  $T_c^{max}$  of the optimally doped samples of the two families  $x = 0.1$  and  $x = 0.4$ . The straight line passes through the origin.

there is a crossing point where it seems that  $E_{max}$  for  $x = 0.4$  becomes smaller than for  $x = 0.1$ . The same situation can be seen for  $T_N$  in the phase diagram of Fig. 1(a). This is another indication that the efficiency of doping holes into the  $\text{CuO}_2$  planes is not the same for the two families. Hence, the two-magnon peak as function of oxygen composition provides a second, independent way of verifying the data collapse method through introducing doping efficiency.

The doping dependence of the two-magnon Raman shift emphasizes the importance of comparing samples with the same effective doping  $\Delta n_{p\sigma}$  and not the same oxygen composition  $y$ . In a recent Raman work on the  $R(\text{Ba,Sr})_2\text{Cu}_3\text{O}_y$  [ $R=(\text{La}, \dots \text{Lu}, \text{Y})$ ], Mallett *et al.* [18] concluded that  $T_c^{max}$  anti-correlates with  $J$ . However, neither the oxygen composition  $y$  nor the number of holes are determined for those samples. In most cuprates  $T_N$  is extremely sensitive to small variations in the oxygen composition, [19] and comparing samples of different compositions can be misleading. In CLBLCO the situation is different; here a region in the phase diagram exists where  $T_N$  is  $y$  independent (see Fig. 1(a)). Therefore, small changes in  $y$  do not affect our conclusions. We suggest that the samples in Ref. [18] have an oxygen composition higher than the crossing point (in Fig. 1(a)), hence the reverse conclusion.

The inset of Fig. 5 summarizes the main finding of this work. In this figure we plot the Raman shift  $E_{max}$  obtained at  $T = 20$  K for the  $x = 0.1$  family (black) and the  $x = 0.4$  family (red) at  $\Delta n_{p\sigma} \approx 0$  versus  $T_c^{max}$  of the crystals. A straight line through the origin is also shown. Although single crystals from only two families are available for this plot, there is clear evidence for a proportionality between the magnetic exchange interaction  $J \simeq E_{max}/3$ , measured by two-magnon Raman scattering, and the superconducting temperature  $T_c^{max}$ . Thus  $T_c^{max} \propto J$  is confirmed by two independent, complementary techniques. The two-magnon Raman scattering technique measures  $J$  directly, but is limited to the antiferromagnetic phase and to single crystals. The analysis of the  $\mu\text{SR}$  technique requires theoretical modeling to extract  $J$ , but it is applicable from the antiferromagnet through the spin glass, and up to the mixed spin-glass superconducting phase.

In the Hubbard model the exchange interaction  $J$  is proportional to  $t^2$ , where  $t$  is hopping rate between neighboring sites.  $t$ , in turn, is determined by overlaps of orbitals on neighboring sites. Our finding indicates that a higher hopping rate corresponds to a larger value of  $T_c$ . This is known as kinetic energy driven superconductivity

scenario. Our data supports the kinetic scenario in the same sense that the isotope effect supports the phonon mediated superconductivity in metals.

This work was supported by the German-Israel Foundation and the joint German-Israeli DIP Project. The authors wish to thank the PSI staff for support with the  $\mu\text{SR}$  experiments and Keun Su Kim for helpful discussions.

- 
- [1] C. A. Reynolds, B. Serin, and L. B. Nesbitt, Phys. Rev. **84**, 691 (1951); B. Serin, C. A. Reynolds, and C. Lohman, Phys. Rev. **86**, 162 (1952); E. Maxwell and O. S. Lutes, Phys. Rev. **95**, 333 (1954).
  - [2] R. Ofer, A. Keren, O. Chmaissem, and A. Amato, Phys. Rev. B **78**, 140508(R) (2008).
  - [3] A. Kanigel, A. Keren, Y. Eckstein, A. Knizhnik, J. S. Lord, and A. Amato, Phys. Rev. Lett. **88**, 137003 (2002).
  - [4] R. Ofer, G. Bazalitsky, A. Kanigel, A. Keren, A. Auerbach, J. S. Lord, and A. Amato, Phys. Rev. B **74**, 220508(R) (2006).
  - [5] A. Knizhnik, Y. Direktovich, G. M. Reisner, D. Goldschmidt, C. G. Kuper, and Y. Eckstein, Physica C **321**, 199 (1999).
  - [6] S. Agrestini, S. Sanna, K. Zheng, R. De Renzi, E. Pusceddu, G. Concas, N. L. Saini, A. Bianconi, Journ. Phys. Chem. Solids **75**, 259 (2014).
  - [7] A. Keren, New J. Phys. **11**, 065006 (2009).
  - [8] E. Amit, A. Keren, Phys. Rev. B **82**, 172509 (2010).
  - [9] see, e.g., H. J. A. Molegraaf, C. Presura, D. van der Marel, P. H. Kes, M. Li, Science **295**, 2239 (2002).
  - [10] G. Drachuck, M. Shay, G. Bazalitsky, R. Ofer, Z. Salman, A. Amato, C. Niedermayer, D. Wulferding, P. Lemmens, A. Keren, J. Supercond. Nov. Magn. **25**, 2331 (2012).
  - [11] S. Sugai, H. Suzuki, Y. Takayanagi, T. Hosokawa, and N. Hayamizu, Phys. Rev. B **68**, 184504 (2003).
  - [12] M. Bloch, J. Appl. Phys. **34**, 1151 (1963); S. R. Chinn, R. W. Davies, and H. J. Zeiger, Phys. Rev. B **4**, 4017 (1971).
  - [13] P. J. Freitas and R. R. P. Singh, Phys. Rev. B **62**, 5525 (2000).
  - [14] P. A. Fleury and R. Loudon, Phys. Rev. **166**, 514 (1968).
  - [15] W. H. Weber and G. W. Ford, Phys. Rev. B **40**, 6890 (1989).
  - [16] A. V. Chubukov and D. M. Frenkel, Phys. Rev. B **52**, 9760 (1995).
  - [17] C. M. Canali and S. M. Girvin, Phys. Rev. B **45**, 7127 (1992).
  - [18] B. P. P. Mallett, T. Wolf, E. Gilioli, F. Licci, G. V. M. Williams, A. B. Kaiser, N. W. Ashcroft, N. Suresh, and J. L. Tallon, Phys. Rev. Lett. **111**, 237001 (2013).
  - [19] see, e.g., S. Sanna, G. Allodi, G. Concas, A. D. Hillier, and R. De Renzi, Phys. Rev. Lett. **93**, 207001 (2004).